Research on Engineering Structures & Materials
www.jresm.org
Research Group

Research Article

Contribution to the micromechanical analysis of compression wave propagation in a granular medium

Said Derbane [*,1,a], Mouloud Mansouri [2,b]

[1]*Department of Civil and Hydraulic Engineering, Faculty of Science and Technology, University of Jijel 18000, Algeria*
[2]*Civil Engineering Research Laboratory of Setif (LRGCS), Department of Civil Engineering, Ferhat Abbas Sétif 1 University, Setif 19000, Algeria*

Article Info

Article History:

Received 21 Nov 2025

Accepted 02 May 2026

Keywords:

Granular medium;
Micromechanical model;
Discrete element method;
Compression wave propagation

Abstract

This paper presents a two-dimensional Discrete Element Method (DEM) investigation of compression wave propagation in a granular soil deposit subjected to a harmonic base excitation. Unlike classical continuum-based approaches, the proposed micromechanical model explicitly accounts for the nonlinearity produced by intergranular interactions. Analysis of the results indicated that the model accurately captures the well-established essential features of the response of a base-excited deposit, such as the motion amplification at the free surface, resonance phenomena, and the degradation of the deformation modulus at large strain levels. Furthermore, the model allowed for the estimation of the strain level at which the degradation of the deformation modulus becomes clearly visible; this level is in good agreement with levels obtained from previous physical experimental work. Furthermore, this study showed that the critical strain value that triggers nonlinear behavior or degradation of deformation moduli is of the same order of magnitude, whether in shear or compression.

1. Introduction

The propagation of mechanical waves in soil deposits is a key topic in earthquake engineering, as it is the mechanism by which seismic motions are transmitted to structures. Classical analyses of wave propagation and site response are predominantly based on continuum mechanics approaches, where soils are idealized as linear or equivalent-linear elastic media. While such methods are effective for cohesive soils and small-strain conditions, they are limited in their ability to represent the nonlinear and discontinuous nature of granular soils. In these materials, stiffness and damping are strain-dependent and controlled by grain-scale mechanisms such as contact deformation, interparticle sliding, and particle rotations. Consequently, when these materials undergo cyclic and dynamic loading, they may exhibit progressive stiffness degradation, excess pore pressure buildup, and, in extreme cases, liquefaction.

The initial experimental studies conducted by Seed et al. [3] laid the basis for understanding soil behavior under cyclic loading and identified a relationship that allows for the estimation of the shear modulus and damping of non-cohesive soils for dynamic analysis, depending on soil type and stress and strain levels, with sands and gravels exhibiting distinct behaviors in terms of stiffness and damping. Subsequent laboratory studies, such as those conducted by Kokusho [2], dealt with cyclic triaxial testing to evaluate dynamic soil properties over a wide strain range. They examined how shear modulus decreases and damping increases with strain level under repeated loading, providing useful data and trends for seismic and dynamic soil analysis.

[*]Corresponding author: said.derbane@univ-jijel.dz, derbane_said@yahoo.fr
[a]orcid.org/0000-0003-7773-5806; [b]orcid.org/ 0000-0002-4179-7488
DOI: http://dx.doi.org/10.17515/resm2026-1356me1121rs

To overcome the limitations of continuum mechanics when applied to granular soils, micromechanical approaches based on the Discrete Element Method (DEM) have been increasingly employed. DEM enables the explicit modeling of individual grains and their interactions, offering direct insight into particle-scale kinematics and force transmission. O'Donovan et al. [4] have conducted an experimental study on a soil model in a cubical cell, they then compared the results with both discrete element (DEM) simulations and continuum modeling. In their study, they used point source transmitters and receivers in order to assess the shear and compression wave velocities in the samples, from which some of the elastic moduli can be deduced. As a result, a satisfactory agreement between experimental observations and DEM simulations is confirmed. Tang and Yang [5] further showed that particle shape significantly affects elastic wave propagation, with angular particles reducing compression wave velocity due to lower coordination numbers and increased interparticle sliding. Similarly, Hu et al. [6] investigated the effect of particle shape on the dynamic behavior of granular soils using the Discrete Element Method. By simulating cyclic undrained triaxial tests under various confining pressures and void ratios, the study showed that angular particles lead to a higher secant shear modulus compared to rounded ones. It has also been shown that, although particle shape has little influence on the modulus ratio (G/G_0), it significantly affects the damping ratio at large strains due to dilatancy. A weighted coordination number is introduced to link particle shape to initial stiffness, and contact sliding is identified as the primary mechanism behind modulus reduction and increased damping.

Yu and Liu [7] developed a micro morphic model that explicitly accounts for particle rotations and local kinematic fluctuations in wave propagation analyses. Zamani and El Shamy [8]. have used discrete element modeling to investigate the vertical propagation of a shear wave in a granular deposit. They looked at the damping ratio and the change in the shear modulus at low frequencies. Using the SHAKE software, the deposit response was estimated as a continuum with linear viscoelastic behavior based on the parameters taken from the DEM simulations. Derbane and Mansouri [20] have analyzed the shear wave propagation in a granular deposit using a discrete element model, they highlighted the degradation of the material's shear modulus and the effect of this degradation on response parameters such as motion amplification and resonance frequency.

DEM simulations are used by Ezzeddine et al. [9] to analyze how sand responds to cyclic triaxial loading by linking macro-scale stress–strain behavior with micro-scale grain interactions. They investigated the effects of cyclic stress level and initial packing density on sand behavior under drained conditions. Macroscopic measures such as shear modulus and damping ratio are examined alongside microscopic indicators like fabric anisotropy, coordination number, friction mobilization, and contact sliding to better understand energy dissipation and structural evolution during cyclic loading.

Despite these advances, most DEM-based studies have focused primarily on shear wave propagation or cyclic shear response. In contrast, compression wave propagation in granular soil remains underexplored. In fact, it is still unclear whether the material properties change with the level of cyclic strain in compression, and whether this evolution is similar in compression as in shear. To address this gap, this study presents an analysis of the propagation of compression waves in granular soil using a 2D discrete-element model. This model simulates a granular deposit composed of circular grains resting on a horizontal bedrock substrate and subjected to vertical harmonic vibration. Particular attention was paid to the amplification of displacement from the base to the surface, taking into account the influence of excitation parameters, namely amplitude and frequency. This model allows for the identification of both the fundamental frequency and the resonance frequency and highlights the gap between them in granular materials, which are intrinsically characterized by a degradation of the modulus of deformation. Overall, this study contributes to a better understanding of the propagation of compression waves in granular media and highlights the limitations of conventional continuum-based approaches.

2. Discrete Element Method for Granular Materials Modeling

The Discrete Element Method (DEM) is particularly well suited for investigating granular materials behavior because it explicitly takes account of the discontinuous nature of such materials. The DEM

formulation is based on the integration of translational and rotational equations of motion for each particle.

2.1. Equations of Grain Motion

The governing equations of motion are expressed as follows [10,11]:

For translational movement

$$m_i\vec{\ddot{x}}_i = \sum_j \vec{F}_{ij}^{contact} + m_i\vec{g} \quad (1)$$

$\vec{\ddot{x}}_i$ is the translational acceleration vector of the grain i, m_i the grain's mass, $\vec{F}_{ij}^{contact}$ is the interaction force applied by a grain j in contact with grain i, $\vec{g}$ the gravity acceleration.

For rotational movement:

$$I_i\vec{\ddot{\varphi}}_i = \sum_j \vec{M}_{ij}^{contact} \quad (2)$$

$\vec{\ddot{\varphi}}_i$ is the rotational acceleration the grain i, I_i is the grain's moment of inertia, $\vec{M}_{ij}^{contact}$ is the torc caused around of the grain i center by the contact forces $\vec{F}_{ij}^{contact}$. Grain interactions occur at contact points, where forces are transmitted through normal and tangential components [12-15], such that:

$$\vec{F}_{ij}^{contact} = \vec{F}_n\vec{n} + \vec{F}_s\vec{s} \quad (3)$$

$\vec{F}_n$ *and* $\vec{F}_s$ are normal and tangential contact forces respectively. The choice of a simple grains shape plays an important role in the optimization of the computation time [15]. The most used shapes are discs for 2D modeling.

2.2. Contact Forces

Interaction forces exist between grains that are in contact. The existence of contact between two grains depends on the normal distance between them (Fig. 1). This distance denoted $\boldsymbol{D_n}$ is defined geometrically by:

$$D_n = \|\vec{x}_j - \vec{x}_i\| - r_i - r_j \quad (4)$$

In which $\vec{x}_i$, $\vec{x}_j$ and r_i, r_j are position vectors and radii of grains i and j, respectively. There is contact if $D_n \leq 0$, this is the contact force calculation condition. The normal contact force is calculated using the viscoelastic model illustrated in Figure 1 and expressed by Eq. 4.

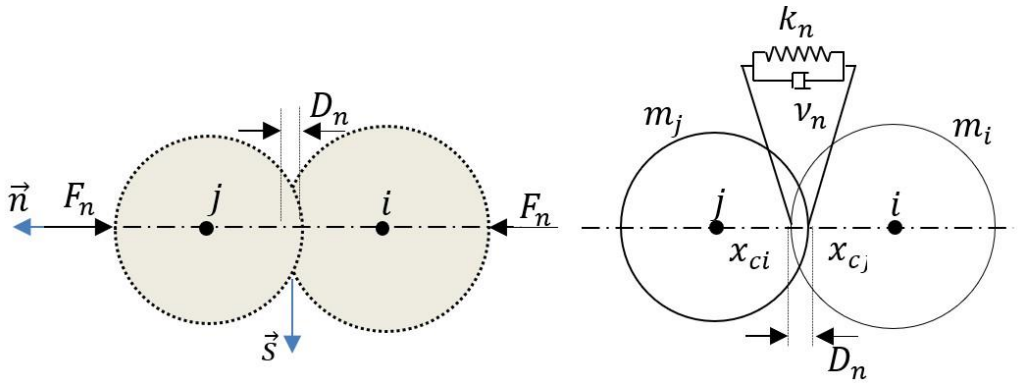

Fig. 1. Normal contact force

$$\vec{F}_n = (-k_n D_n - v_n V_n).\vec{n} \quad (5)$$

Where k_n and v_n are the elastic constant and viscous damping constant respectively and V_n is the normal velocity of grain j with respect to grain i. The tangential contact force between two grains

is computed through a viscoelastic model with friction illustrated in Figure 2 and expressed by Eq. 6.

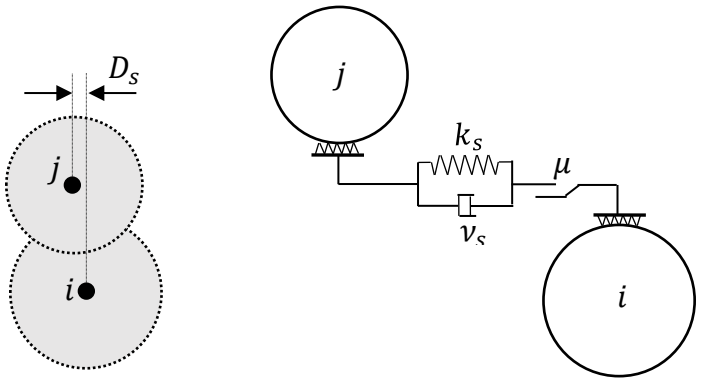

Fig. 2. Shear contact force between grains

$$F_s = min(k_s D_s + v_s V_s,\ \mu_d F_n) \tag{6}$$

Where k_s is the tangential stiffness, v_s the viscous damping coefficient, μ_d is the inter-particle coefficient of friction, D_s is the grain deformation due to shear force. V_s is the tangential velocity of grain j with respect to grain i. $\mu_d F_n$ is the Coulomb dynamic threshold; if the viscoelastic tangential force $k_s D_s + v_s V_s$ exceeds $\mu_d F_n$, a slip occurs in the contact.

When using circular shaped grains, it is often interesting to introduce rolling resistance in order to mimic the rotational hindrance observed in natural granular soils. In this work, the rolling resisting moment is assumed to result from the eccentricity of the normal contact force as illustrated in figure 3[17], therefore, it is computed as follows:

$$M_r = F_n . b_r \tag{7}$$

Where b_r is the rotational arm. $b_r = \alpha . \beta,\ \beta = \sqrt{r^2 - (r + \frac{D_n}{2})^2}$, $0 < \alpha < 1$ in this work α is fixed to 0.5.

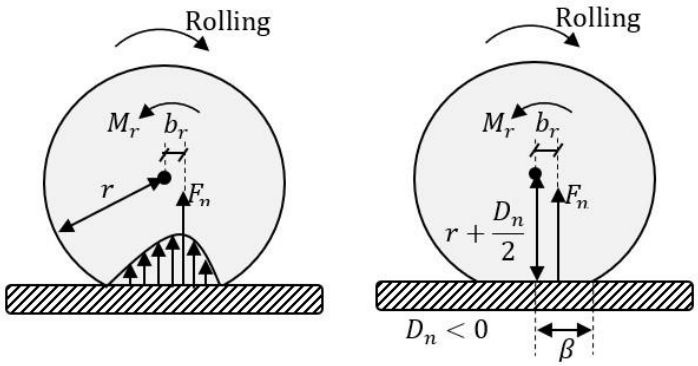

Fig. 3. Rolling resistance model

2.3. Contact Duration and Time Step Integration

The equations of motion governing the translational and rotational dynamics of each particle are solved using an explicit time integration scheme. In this study, a velocity-Verlet algorithm is adopted due to its widespread use in DEM simulations and its ability to ensure numerical stability. The integration scheme updates particle positions, velocities, and rotations at each time step based on the resultant contact forces and moments.

In discrete element modelling, the calculation stability is related to the precise resolution of the contact duration t_c. The integration time step (Δt) must therefore be sufficiently small compared

to the contact duration. A common practice is to set $\Delta t \approx t_c/10$. For a linear viscoelastic contact model, the contact duration t_c can be approximated as:

$$t_c = \pi\sqrt{\frac{m_{eff}}{k_n}} \tag{8}$$

Where $m_{eff} = \frac{m_i.m_j}{m_i+m_j}$ is the effective mass and k_n is the normal stiffness? Accordingly, the maximum allowable time step is given by:

$$\Delta t_{max} \approx 0.1\pi\sqrt{\frac{m}{k_n}} \tag{9}$$

Where; m is the system's smallest effective mass.

3. Analytical Solution of Compression Wave Propagation in Elastic Deposits

The analytical solution is presented here as described in reference [18]. The soil deposit is modeled as a one-dimensional, homogeneous, linear elastic layer subjected to vertical compression-wave propagation. The base of the layer is assumed to be rigid and excited by a prescribed harmonic displacement, while the top boundary is considered stress-free, representing a free surface. These boundary conditions are selected to ensure consistency between the analytical solution and numerical model.

The vertical displacement $u(z,t)$ that depends on the vertical coordinate z and tile t is governed by the differential equation:

$$V_p^2\frac{\partial^2 u}{\partial z^2} = \frac{\partial^2 u}{\partial t^2} \tag{10}$$

Where; V_p is the compression wave propagation velocity having the expression:

$$V_p = \sqrt{\frac{E}{\rho}} \tag{11}$$

Where E is the modulus of deformation and ρ is the mass density. Note that for a 1D solid, E represents the material's modulus of elasticity in this expression, but for a soil layer considered horizontally infinite, horizontal deformation is prevented; consequently, E represents the oedometer modulus.

When the soil layer of thickness h is subjected to a harmonic excitation at the base of the form $u_0 \sin \omega t$, the solution of the wave equation is:

$$u(z,t) = -\frac{u_0 V_p}{E\omega}\frac{(\sin\frac{\omega}{V_p}(h-z))}{\cos(\frac{\omega}{V_p}h)}.\sin\omega t \tag{12}$$

4. Modeling of Compression Wave Propagation in A Soil Deposit

In this study, a two-dimensional discrete element method (DEM) is employed to simulate the propagation of compression wave in a granular soil deposit. Soil grains are deposited under gravity to form a dense granular assembly. The used boundary conditions are: (1) periodic boundaries in the horizontal direction; this choice eliminates spurious wave reflections from vertical boundaries and allows to represent an infinitely extended soil layer in the horizontal direction, (2) stress free for the top surface of the deposit and (3) controlled displacement for the base surface representing the bedrock, a chain of grains is bonded to this bedrock to limit the sliding of the deposit grains over it. To simulate the behavior of deeper soil layers, it is possible, as an option, to apply a vertical load to the upper surface by means of a chain of grains of prescribed weight (see Fig. 4b).

The excitation is generated by applying a vertical harmonic displacement to the bedrock. The soil deposit is discretized into several horizontal layers. The average displacement within each layer corresponds to the average displacement of all the grains belonging to that layer. The average

displacements of all layers are recorded throughout the excitation to evaluate the wave transmission characteristics.

5. Results of Numerical Simulations and Discussion

5.1. DEM Model Parameters

Figure 4 illustrates the soil granular profile model subjected to excitation, along with the applied boundary conditions. The physical properties of the particles and the micromechanical parameters used to compute contact forces are summarized in Table 1.

Table 1. Simulation parameters [19- 21]

Parameters	Value
Number of Grains	5000
Grains radius r_i	$1.00\text{x}10^{-3}$ to $2.00\text{x}10^{-3}m$
Density ρ	2600 kg/m^3
Normal intergranular stiffness k_n	$1.2\ \text{x}10^{6}N/m$
Shear intergranular stiffness k_s	$9.6\text{x}10^{5}N/m$
Intergranular friction coefficient μ	0.5
Normal viscous damping coefficient v_n	41.38 kg/s
Tangential viscous damping coefficient v_s	33.10 kg/s
Acceleration of gravity g	9.81 m/s^2

The number of grains used in this model (5,000 grains) represents a compromise between using a representative unit volume and computational cost. The radii (r_i) and density (Gs) correspond approximately to natural sand of medium grain size. The stiffnesses k_n and k_s are often reduced relative to their natural values in order to allow for a reasonable time step (Δt). The ratio $\frac{k_n}{k_s} = 0.8$ is commonly adopted in DEM simulations and reflects typical contact behavior between granular. The interparticle friction coefficient ($\mu = 0.5$) corresponds to the values widely reported for dense granular materials and ensures a realistic level of interparticle sliding. The normal and tangential damping coefficient (v_n and v_s) were selected to ensure numerical stability while preserving the dynamic response of the system without introducing excessive damping [10, 12, 19, 20, 27].

The granular deposit used for the compression-wave propagation analyses consist of 5000 circular particles whose diameters follow the size distribution proposed by Voivret et al. [25]. The particle radii range from $1.00\text{x}10^{-3}$ to $2.00\text{x}10^{-3}m$. The granular deposit is generated by gravitational pluviation. At the initial stage, grains are placed on a regular lattice with no interparticle contact, then they are released under gravity, allowing them to settle onto the rigid base representing the bedrock (Fig. 4a). Once the assembly reaches mechanical equilibrium, the resulting grains positions are recorded and used as the reference positions for the subsequent dynamic simulations. During the compression-wave propagation tests, the displacement field is obtained by tracking the evolution of particle positions relative to their reference coordinates at each time step.

It should be noted that the initial void ratio depends on several parameters, including the interparticle friction coefficient and the pluviation procedure (initial particle arrangement and spacing). In order to obtain a dense deposit, the intergranular friction coefficient is set to zero during deposition, and grains are initially arranged according to a lattice (Fig. 4a). After deposition and stabilization, the friction coefficient to be used in the dynamic simulations is applied. The width of the deposit being set at 2m, the height after deposition is 0.54m (Fig. 4b). The harmonic displacement excitation is prescribed as $u(t) = u_0 \sin(\omega t)$, where u_0 is the displacement amplitude and ω denotes the circular frequency.

To minimize the effects of transient responses of soil deposit, the excitation is applied in three phases, following the approach outlined in reference [8, 20]. In the first phase, the amplitude of excitation is gradually increased from zero to the target steady-state value. During the second phase, the amplitude is held constant to induce a steady-state oscillation. Finally, in the third phase, the amplitude is progressively reduced back to zero. In the simulations presented, the durations of

these three phases are set to 4.5 seconds, 6 seconds, and 1.5 seconds, respectively. This staggered loading strategy ensures that transient effects are significantly dampened during the steady-state vibration phase. The results discussed hereafter correspond primarily to this steady-state phase. For analysis purposes, the soil deposit is subdivided in this work, into seven (7) horizontal layers, and the displacement recorded in each layer represents the average displacement of all grains contained within that layer.

(a)

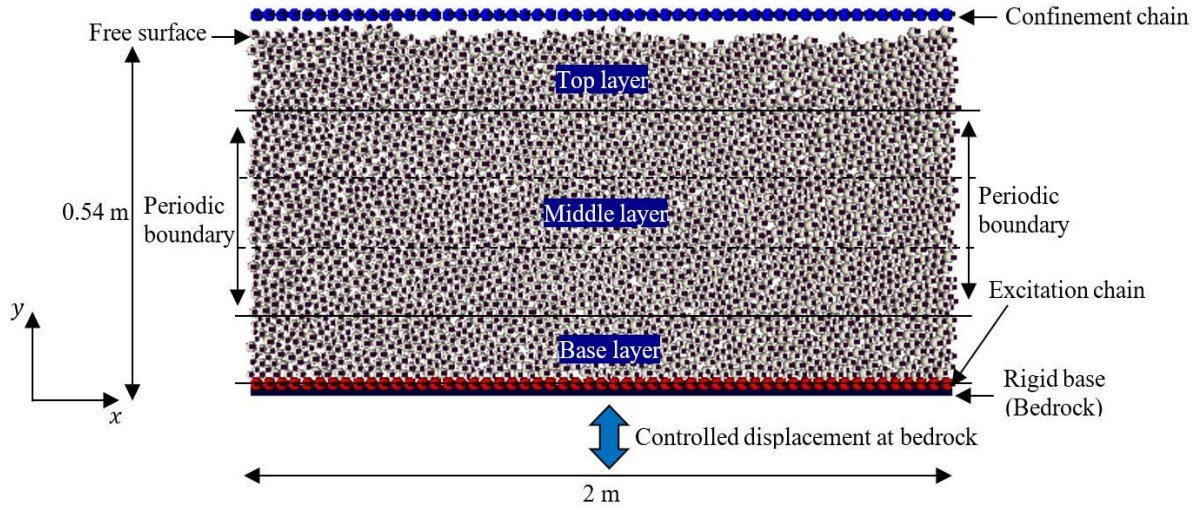

(b)

Fig. 4. (a) The grain positions before pluviation under gravity and (b) The granular deposit and boundary condition [20]

5.2. Displacement Response and Amplification of Movement

In this analysis, the excitation parameters are $u_0 = 4 \times 10^{-4} m$ and $\omega = 30\ rad/s$. In the first phase (i.e., from 0 to 4.5 s), the displacement amplitude is increased proportionally to time from zero to $4 \times 10^{-4}\ m$. It is then maintained at the same amplitude for $6s$, then gradually decreased to zero over 1.5 s. Figure 5 shows the resulting displacement response at two locations: the bedrock (Fig. 5a) and the top layer of the soil profile (Fig. 5b).

Figure 5c shows the displacement time history for part of the steady-state vibration phase at the centers of the different layers. The change in vibration amplitudes with distance from the base of the deposit is plotted in figure 5d. These figures show that motion amplification increases progressively from the base to the top of the soil deposit. Moreover, Figure 5d displays a

displacement pattern characteristic of the first vibration mode, indicating that the excitation frequency is lower than the fundamental frequency of the deposit [27].

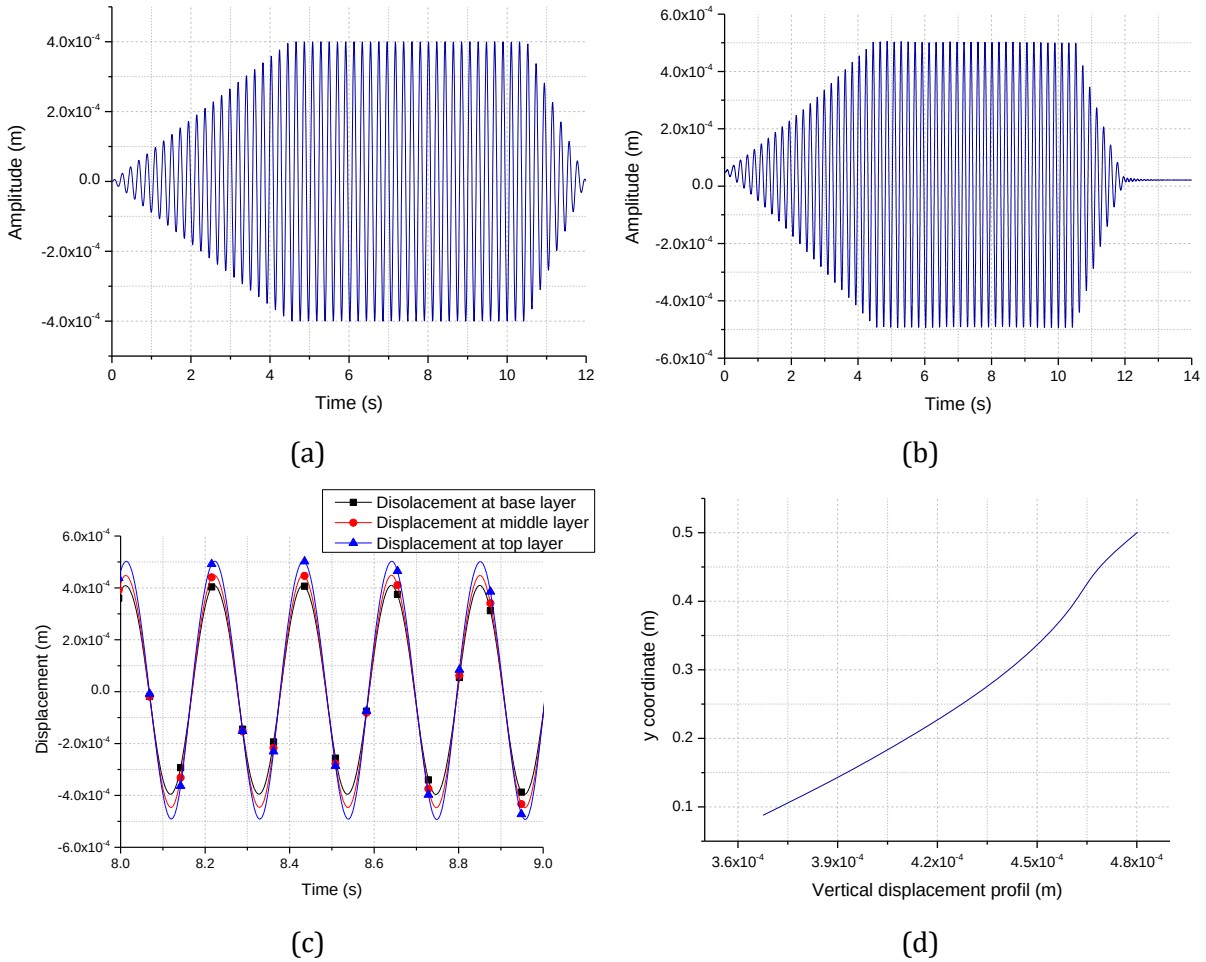

Fig. 5. Displacement response: (a) Displacement time history at the bedrock (excitation), (b) Displacement time history at the top layer of the soil deposit, (c) Displacement time history at different depths in a part of the steady-state phase, (d) Vertical displacement profile vs. y coordinate

5.3. Equivalent Linear Elastic Continuum Model

This section consists of an inverse analysis to determine the properties of a linear elastic soil profile equivalent to the sand deposit under study. This analysis provides a better understanding of the behavior of the deposit under different vibration amplitudes and highlights the limitations of the analytical model based on continuum theory with linear elastic behavior in the modeling of deposits composed of naturally discontinuous materials such as sands. For consistency, the analytical model used has the same geometric dimensions as those adopted in the DEM model.

The analytical solution for the displacement of an elastic deposit subjected to harmonic excitation at the base is given by Eq. 12. This analysis aims to determine the wave propagation velocity (V_p) to be used in this solution, such that the vibration amplitude at the free surface matches that obtained from the discrete-element model. The analysis examines four base excitation amplitudes, three moderate amplitudes and one large amplitude, specifically $u_0 = 2 \times 10^{-4}m$, $u_0 = 4 \times 10^{-4}m$, $u_0 = 8 \times 10^{-4}$m and $u_0 = 8 \times 10^{-3}m$. In all cases, the excitation frequency is kept constant at $30rad/s$.

Figure 6 shows the time history displacement in the steady-state vibration phase for the four applied amplitudes. For excitation amplitudes $2 \times 10^{-4}m$, $4 \times 10^{-4}m$ and $8 \times 10^{-4}m$ (figures. 7a, 6b and 6c), the numerical displacement and the analytical solution calibrated with the wave

propagation velocity V_p are presented on the same graphs. For excitation amplitude $8 \times 10^{-3}m$ (Fig. 6d), only the numerical displacement is shown, as the analytical solution does not allow obtaining such numerical displacement shape.

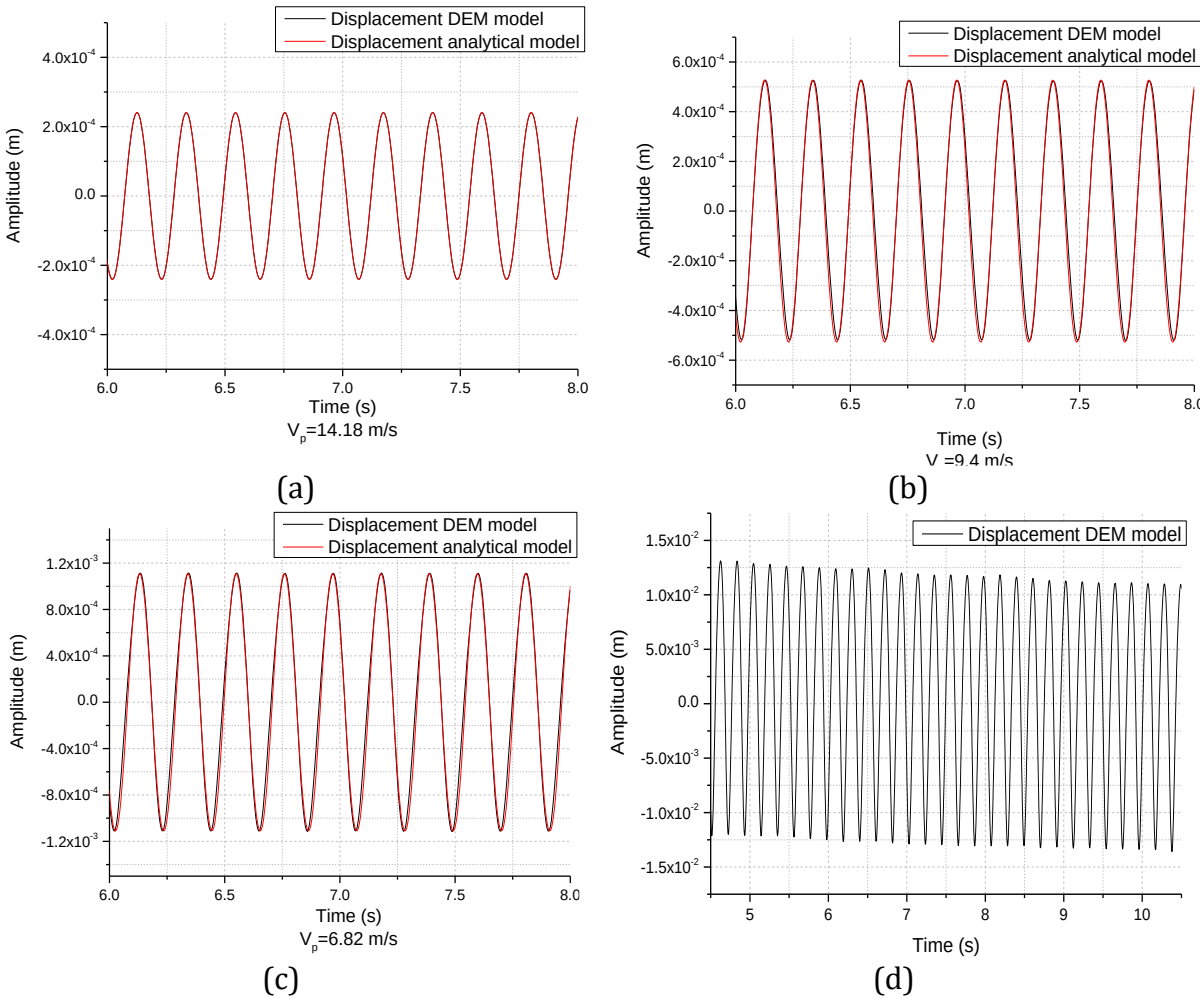

Fig. 6. Displacements at the free surface layer from the DEM model and calibrated analytical solution with different excitation amplitude: (a) $u_0 = 2 \times 10^{-4}m$, (b) $u_0 = 4 \times 10^{-4}m$, (c) $u_0 = 8 \times 10^{-4}m$, (d) $u_0 = 8 \times 10^{-3}m$

The wave propagation velocities (V_p) determined so that the analytical solution yields displacement amplitudes similar to those of the numerical model are $14.18m/s$, $9.4m/s$ and $6.82m/s$ respectively, for excitation amplitudes of $2 \times 10^{-4}m$, $4 \times 10^{-4}m$ and $8 \times 10^{-4}m$. The material's modulus of elasticity can be calculated from the wave propagation velocity (V_p) using Eq. 11. The density (ρ) in this equation can be regarded as the average density of the deposit, calculated as the ratio of the total mass of the grains to the volume of the deposit; it is approximately $\rho = 1996.77kg/m^3$. The elastic moduli of the equivalent linear elastic deposits, corresponding to the three excitation amplitudes of $2 \times 10^{-4}m$, $4 \times 10^{-4}m$ and $8 \times 10^{-4}m$, are $401.49 \times 10^3 Pa$, $176.43 \times 10^3 Pa$ and $92.87 \times 10^3 Pa$, respectively. This result shows that the equivalent linear elastic model becomes more flexible as the excitation amplitude increases, indicating that the deposit exhibits increasingly soft behavior at larger strains. This result is consistent with experimental observations on the cyclic behavior of granular soils, where the moduli of deformation decrease as the strain level increases [2,3,20]. For the large amplitude, i.e. $u_0 = 8 \times 10^{-3}m$, in addition to a more pronounced amplification of surface displacement, harmonic oscillation is maintained but around a downward-sloping mean line; this observation indicates that, at this amplitude level, a deposit densification process is triggered, which causes the surface layer to shift downward.

5.4. Fundamental Frequency of The Deposit

The fundamental frequency (first natural frequency) of the deposit, is estimated in this work from the free oscillation observed after the excitation stops. This vibration has a very low amplitude, so it can be assumed to be a damped elastic vibration. Figure 7 shows the free vibration displacement in the top layer after the excitation has ended. The maximum displacement amplitude applied during the excitation phase is $4 \times 10^{-4} m$. The free oscillation period of the deposit can be estimated directly from this plot and is about $T = 0.1054\ s$. The circular fundamental frequency is therefore: $\omega_1 = \frac{2\pi}{T} = 59.62 rad/s$.

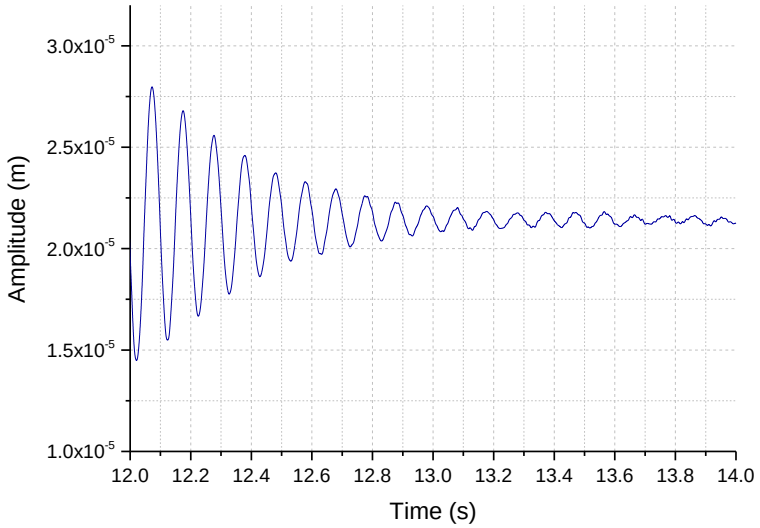

Fig. 7. Detailed view of response at the top layer during free vibration

The compression wave velocity can be estimated using the fundamental period through the relation $V_p = \frac{4h}{T}$ [19]. Accordingly, for our deposit model: $V_p = 20.49 m/s$. The corresponding modulus of elasticity, calculated using Eq. 11, is $838.32 \times 10^3 Pa$; this is the maximum modulus of elasticity, which is characteristic of the material's behavior under very small strains. Once again, this result clearly confirms the concept of degradation of deformation modulus. Indeed, it can be observed that the moduli obtained in the inverse analysis performed earlier (in the previous section), are all lower than the maximum modulus calculated based on very small deformations.

5.5. Resonance Frequency of The Deposit

The resonance frequency is estimated based on a frequency sweep, in which the excitation frequency is gradually varied to detect resonance. This frequency should be theoretically, very close to the fundamental frequency for sufficiently low amplitudes. Figure 8 shows the variation in displacement amplification during steady-state vibration, as a function of excitation frequency ranging from $\omega = 20\ rad/s\ to\ 65\ rad/s$. Amplification is quantified here by the ratio (u/u_0), where u_0 is the excitation amplitude at the base, taken as $4 \times 10^{-4} m$ in this case.

It is clear that the amplification ratio follows the typical trend observed in elastic systems subjected to harmonic excitation i.e., as the excitation frequency increases, the amplification gradually increases, reaches a peak at resonance, and then decreases. The resonance frequency identified from the graph is approximately $57\ rad/s$. This frequency is slightly lower than the fundamental frequency estimated above, which may be due to two parameters, namely: (1) the presence of damping introduces a shift between the natural frequency and the resonance frequency, and (2) the possible degradation of the deformation modulus due to large strains during resonance.

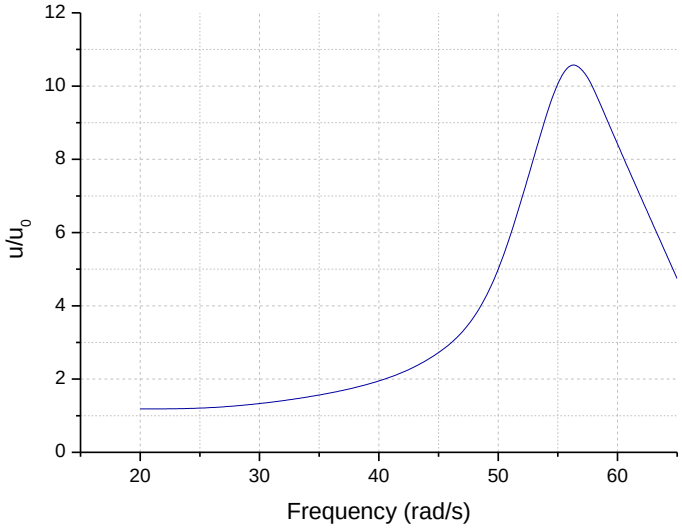

Fig. 8. Displacement amplification vs. excitation frequency

5.4. Influence of Strain Level on Displacement Amplification

It is worth recalling that, for an elastic deposit subjected to harmonic excitation, the dynamic amplification ratio at the free surface (u/u_0) is theoretically independent of the excitation amplitude. However, since, in most cases, a granular material does not exhibit purely elastic behavior, it is important to study the response of the deposit to different levels of strain. To this end, the specimen is subjected to a harmonic excitation with the shape described above, with a fixed frequency of 30 rad/s and different amplitudes ranging from $4 \times 10^{-6}\ m$ to $3 \times 10^{-3}\ m$.

For frequency excitation of $30\ rad/s$, the displacement profile is nearly linear (Fig. 5d), which allows the vertical normal strain (ε_c) to be approximated by the ratio of the difference in vertical displacement between two layers to their vertical spacing. To estimate average value over the deposit, we used here the penultimate layer (layer 6) and the second layer. Therefore, the average vertical strain is expressed as:

$$\varepsilon_y = \frac{u_6^p - u_2}{y_6 - y_2} \tag{11}$$

In this expression, u_6^p represents the peak displacement of layer 6, u_2 the displacement of layer 2 at the same instant (corresponding to u_6^p), and y_i the vertical coordinate of the center of layer i. Average vertical strain levels are computed for all excitation amplitudes in the steady-state vibration phase.

Figure 9a shows how the level of vertical normal strain varies with excitation amplitude; the axes of the graph are plotted on a logarithmic scale to accommodate the wide range of values. This graph shows that the strain level increases as the excitation amplitude goes up. As for the rate of change, although it is nearly constant, it shows a slight increase as the excitation amplitude gets higher. Figure 9b displays the evolution of the displacement amplification ratio at the free surface (u/u_0) as a function of the vertical strain level induced by different excitation amplitudes. This graph shows that the amplification remains nearly constant for small strains ($\varepsilon_y \leq 4 \times 10^{-5}$). This observation indicates that below this strain level, the deposit behaves almost like a linear elastic medium. Above this strain level, the amplification increases with strain; this may be explained by the tendency of the deposit to become increasingly soft as the strain level increases. This tendency could be attributed to the onset of nonlinear behavior caused by intergranular slippage and grain rotation.

It is worth noting that the critical strain value—which separates the two types of behavior (linear and nonlinear)—obtained in this study is about $\varepsilon_y \approx 4 \times 10^{-5}$ (see Fig. 9b). Besides, Kokusho [2], in his experimental study on the cyclic behavior of soils using the triaxial device, has obtained the

degradation curve of the deformation modulus shown in Figure 10. It can observe on this curve, that the critical strain, which marks the effective degradation of the deformation modulus, is on the order of 5×10^{-5}. It is therefore clear that the critical strain level corresponding to the onset of degradation of the deformation modulus in the present numerical study is in good agreement with Kokusho's experimental result.

Finally, this study showed that the degradation of the oedometeric deformation modulus under cyclic loading is similar to that of the shear modulus. Furthermore, the critical strain value that triggers the effective degradation of the oedometeric modulus is of the same order as that corresponding to the shear modulus, which is on the order of 10^{-5} to 10^{-4} [2,3,20,28].

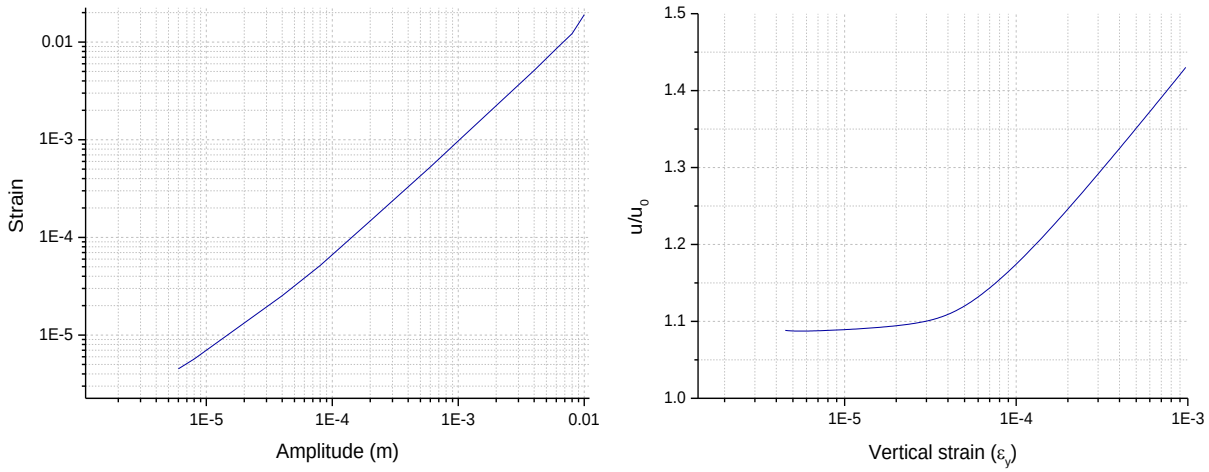

(a) (b)

Fig. 9. (a) Average vertical normal strain level vs. excitation amplitude; (b) Displacement amplification ratio vs. vertical normal strain induced by various excitation amplitudes

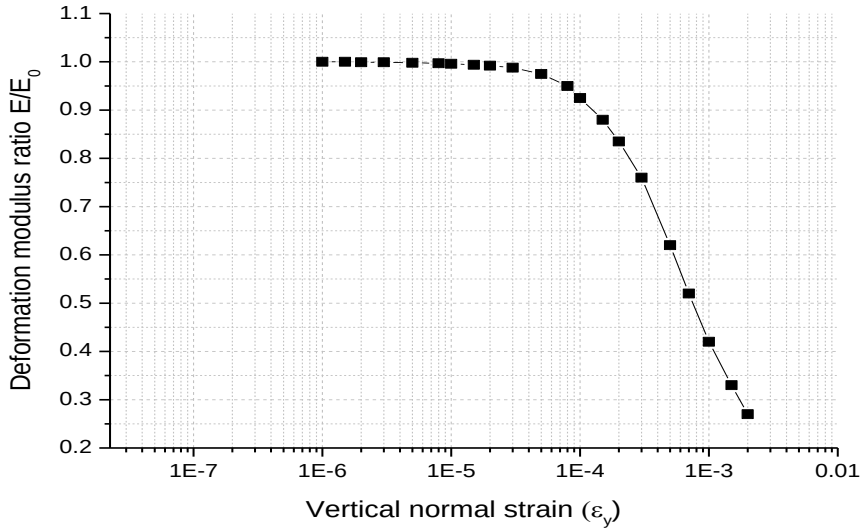

Fig. 10. Soil deformation modulus degradation under cyclic loading.
Obtained by Kokusho [2] from cyclic triaxial tests

6. Conclusions

This work aimed to investigate the mechanisms involved in the propagation of compression waves in a soil deposit at different strain levels. To this end, we analyzed the propagation of compressional motion in a granular deposit excited at its base by a sinusoidal vertical motion. The problem is approached using the 2D discrete element model. The boundary conditions used are a controlled displacement condition at the base, a free boundary on the top surface, and periodic type boundaries on the lateral vertical boundaries to model the infinite aspect of the deposit's horizontal dimension.

This study first allowed us to evaluate the fundamental frequency and the maximum deformation modulus corresponding to a low level of deformation. Secondly, it was shown that for excitation frequencies below the fundamental frequency, the motion is amplified from bottom to top up to the free surface, meaning that the vibration occurs in the first mode. The inverse analysis performed showed that for moderate excitation amplitudes, it is possible to determine a linear elastic model equivalent to the granular deposit. It was observed that the equivalent elastic deformation modulus decreases with increasing amplitude. However, for high amplitudes, it was not possible to obtain an equivalent elastic model due to the densification of the deposit during vibration. Analysis of the amplification evolution as a function of excitation amplitude, and consequently as a function of strain level, showed that for low strain levels, the amplification is almost constant. However, beyond a certain critical strain value, the amplification increases with increasing strain amplitude. The value of this critical strain is in very good agreement with that which triggers the degradation of the deformation modulus, a phenomenon well-known in the literature. Furthermore, it is noted that this value, which corresponds to compressive stress, is of the same order of magnitude as that of shear stress.

Appendix: Table of symbols

Symbol	Definition	Description	Unit
$\vec{x}_i$	Position vector	Position of grain i	m
$\ddot{\vec{x}}_i$	Acceleration vector	Translational acceleration of grain i	m/s^2
$\vec{\varphi}_i$	Rotation vector	Angular displacement of grain i	rad
$\ddot{\vec{\varphi}}_i$	Angular acceleration	Rotational acceleration of grain i	rad/s^2
m_i	Mass	Mass of grain i	kg
I_i	Moment of inertia	Moment of inertia of grain i	kg·m^2
$\vec{F}_{ij}^{contact}$	Contact force	Force exerted by grain j on grain i	N
$\vec{F}_n$	Normal contact force	Normal component of contact force	N
$\vec{F}_s$	Tangential contact force	Tangential component of contact force	N
D_n	Normal overlap	Normal contact overlap between grains	m
D_s	Tangential displacement	Accumulated tangential displacement	m
V_n	Normal relative velocity	Normal relative velocity at contact	m/s
V_s	Tangential relative velocity	Tangential relative velocity at contact	m/s
k_n	Normal stiffness	Normal contact stiffness	N/m
k_s	Tangential stiffness	Tangential contact stiffness	N/m
v_n	Normal damping coefficient	Viscous damping coefficient in normal direction	kg/s
v_s	Tangential damping coefficient	Viscous damping coefficient in tangential direction	kg/s
μ_s	Static friction coefficient	Static interparticle friction coefficient	–
μ_d	Dynamic friction coefficient	Dynamic interparticle friction coefficient	–
M_r	Rolling resistance moment	Moment resisting rolling at contact	N·m
$u(z,t)$	Displacement	Vertical displacement at depth z and time t	m
u_0	Excitation amplitude	Amplitude of applied harmonic displacement	m
ω	Angular frequency	Excitation circular frequency	rad/s
E	Oedometric modulus	Dynamic compression modulus of soil	Pa
ρ	Density	Bulk density of granular soil	kg/m^3
h	Soil layer depth	Total thickness of the soil deposit	m

References

[1] Wichtmann T, Triantafyllidis T. Mechanical behaviour of soils under environmentally-induced cyclic loads. Berlin: Springer Science & Business Media; 2012. p. 1-136. https://doi.org/10.1007/978-3-7091-1068-3_1

[2] Kokusho T. Cyclic triaxial test of dynamic soil properties for wide strain range. Soils and Foundations. 1980;20(2):45-60. https://doi.org/10.3208/sandf1972.20.2_45

[3] Seed HB, Wong RT, Idriss I, Tokimatsu K. Moduli and damping factors for dynamic analyses of cohesionless soils. J Geotech Eng. 1986;112(11):1016-1032. https://doi.org/10.1061/(ASCE)0733-9410(1986)112:11(1016)

[4] O'Donovan J, Ibraim E, O'sullivan C, Hamlin S, Muir Wood D, Marketos G. Micromechanics of seismic wave propagation in granular materials. Granular Matter. 2016;18:1-18. https://doi.org/10.1007/s10035-015-0599-4

[5] Tang X, Yang J. Wave propagation in granular material: what is the role of particle shape?. Journal of the Mechanics and Physics of Solids. 2021;157:104605. https://doi.org/10.1016/j.jmps.2021.104605

[6] Hu J, Wu H, Gu X, Zho Q. Particle shape effects on dynamic properties of granular soils: A DEM study. Computers and Geotechnics. 2023;161:105578. https://doi.org/10.1016/j.compgeo.2023.105578

[7] Yu P, Liu Y. Micromorphic modeling of wave propagation in granular materials: Considering particle nonaffine micro-deformation and kinematics decomposition. Powder Technology. 2022;411:117919. https://doi.org/10.1016/j.powtec.2022.117919

[8] Zamani N, El Shamy U. Analysis of wave propagation in dry granular soils using DEM simulations. Acta Geotechnica. 2011;6:167-182. https://doi.org/10.1007/s11440-011-0142-7

[9] Ezzeddine A, Cazacliu B, Richard P, Thorel L, Artoni R. A discrete element study on sand response to cyclic loading: macro-micro perspectives. Granular Matter. 2024;26(4):101. https://doi.org/10.1007/s10035-024-01467-7

[10] Pöschel T, Schwager T. Computational Granular Dynamics - Models and Algorithms. Berlin Heidelberg: Springer-Verlag; 2005.

[11] Mansouri M, El Youssoufi MS. Numerical simulation of the quicksand phenomenon by a 3D coupled Discrete Element - Lattice Boltzmann hydromechanical model. Int J Numer Anal Meth Geomech. 2016. https://doi.org/10.1002/nag.2556

[12] Cundall PA, Strack OA. A discrete numerical model for granular assemblies. Geotechnique. 1979;29(1):47-65. https://doi.org/10.1680/geot.1979.29.1.47

[13] Cundall PA, Hart RD. Numerical modelling of discontinua. Engineering Computations. 1992;9(2):101-113. https://doi.org/10.1108/eb023851

[14] Richefeu V. Approche par éléments discrets 3D du comportement de matériaux granulaires cohésifs faiblement contraints [Doctoral dissertation]. Université Montpellier II-Sciences et Techniques du Languedoc; 2005.

[15] Delenne JY, El Youssoufi MS, Cherblanc F, Bénet JC. Mechanical behaviour and failure of cohesive granular materials. International Journal for Numerical and Analytical Methods in Geomechanics. 2004;28(15):1577-1594. https://doi.org/10.1002/nag.401

[16] Fakih M, Delenne JY, Radjai F, Fourcaud T. Root growth and force chains in a granular soil. Phys Rev E. 2019;99(4):042903. https://doi.org/10.1103/PhysRevE.99.042903

[17] Saidani D, Mansouri M, Khellaf A. Analysis of the preloading effect on shear strength for dense sandy soils A discrete element modeling. Innovative Infrastructure Solutions. 2022;7(1):81. https://doi.org/10.1007/s41062-021-00680-0

[18] Verruijt A. An introduction to soil dynamics. Vol. 24. Springer Science & Business Media; 2009.

[19] Luding S. Cohesive, frictional powders: contact models for tension. Granular Matter. 2008;10(4):235-246. https://doi.org/10.1007/s10035-008-0099-x

[20] Derbane S, Mansouri M, Messast S, El Malki Alaoui A. On the behavior of a granular soil deposit subjected to horizontal vibration. A discrete element modeling. Comptes Rendus Mécanique. 2025;353:321-338. https://doi.org/10.5802/crmeca.282

[21] Derbane S, Mansouri M, Messast S. Contribution to micromechanical modeling of the shear wave propagation in a sand deposit. Technology Audit and Production Reserves. 2024;3(1(77)):10-18. https://doi.org/10.15587/2706-5448.2024.301709

[22] Iwasaki T, Tatsuoka F, Takagi Y. Shear moduli of sands under cyclic torsional shear loading. Soils and Foundations. 1978;18(1):39-56. https://doi.org/10.3208/sandf1972.18.39

[23] Fu L, Zhou S, Zheng Y, Zhuang L. Characterizing dynamic load propagation in cohesionless granular packing using force chain. Particuology. 2023;81:135-143. https://doi.org/10.1016/j.partic.2023.01.007

[24] Kim DS, Stokoe II KH. Characterization of resilient modulus of compacted subgrade soils using resonant column and torsional shear tests (with discussion and closure) (No. 1369). Transportation Research Record; 1992.

[25] Voivret C, Radjaï F, Delenne JY, El Youssoufi MS. Space-filling properties of polydisperse granular media. Phys Rev E. 2007;76(2):021301. https://doi.org/10.1103/PhysRevE.76.021301
[26] Zhou WH, Yin ZY. Practice of discrete element method in soil-structure interface modelling. Springer; 2022. https://doi.org/10.1007/978-981-19-0047-1
[27] Rouabeh A, Aouari I, Benahmed B, Palanci M. Improved PGA and PGV estimation in soft soils for earthquake engineering applications. Res Eng Struct Mater. 2025;11(6):3167-3186. https://doi.org/10.17515/resm2025-857ea0429rs
[28] Sun S, Zhu D, Zhang Z. Experimental study on the compression characteristics of sandy soil under impact loading. Res Eng Struct Mater. 2025;11(2):903-920. https://doi.org/10.17515/resm2025-586me1223rs